Available online at www.sciencedirect.com
SCIENCE DIRECT®
Journal of Magnetic Resonance 176 (2005) 79–86
JMR Journal of Magnetic Resonance
www.elsevier.com/locate/jmr

A novel high temperature ^{1}H NMR imaging probe for combustion studies: The behaviour of both a lit and unlit methane gas jet

P.M. Glover [b,*], B. Newling [a], C. Poirier [a], B.J. Balcom [a]

[a] Physics Department, University of New Brunswick, NB, Canada E3B 5A3
[b] School of Physics and Astronomy, University of Nottingham, Nottingham NG7 2RD, UK

Received 16 March 2005; revised 9 May 2005
Available online 23 June 2005

Abstract

The design of a NMR probe suitable for very high temperature samples is described. The loop gap resonator is water cooled and tuned to 100 MHz for use in a 2.4 T horizontal bore magnet. The probe has been specifically designed for imaging of the combustion process. An experiment is described in this paper which shows the behaviour of a methane gas jet when both lit and unlit. The jet of gas may be observed in its unlit state flowing at up to 2 m s^{-1} from a 1 mm diameter orifice using a Single Point Imaging technique. Images of the lit gas show loss of nuclear polarisation within 3 mm of the orifice. A residual amount of un-decomposed gas is visible in the first few millimetres of the flame neck. A computational fluid dynamics model is used to verify the distribution of molecular methane, as well as the temperature of the flame.

Keywords: SPRITE; Single-point imaging; Gas flow; Gas combustion; Flame

1. Introduction

There is much interest in the process of combustion as it is the primary way in which chemical energy is harnessed. In many applications, there is a subsequent conversion to other forms of energy (electrical or mechanical). In all cases, an efficient conversion is desired. The magnetic resonance techniques can contribute greatly to the investigation of combustion. NMR and MRI can analyse and visualise the fuel components—solid, liquid, and gas. In addition, they can monitor the formation of combustion products, but usually separately from, and when cooler than the combustion process [1]. NMR methods are also capable of quantifying flow, as well as temperature and composition [2]. ESR is able to monitor the radicals liberated during thermal decomposition of the fuel. Spatial distribution of these radicals may be determined by moving a large flame up and down through a cavity [3]. Model predictions and invasive sampling measurements [4] together with other techniques (fluoroscopy for example [5]) show a distribution of un-decomposed hydrocarbon within the body of a flame. MRI should be able to detect these protons in situ even though the temperature is approaching 500 K just a few millimetres into the flame. Temperature measurements on large flames are carried out routinely, although these, like sampling, are invasive. Flow is also determined by particle velocimetry [6]. Detailed descriptions, models, and temperature of hydrocarbon combustion are available in these articles and other literature and are not discussed further in any detail here.

Computational Fluid Dynamics software has been corroborated by MRI flow measurements in a number of experiments for both liquid and gas phases [7,8].

* Corresponding author. Fax: +44 115 9515166.
E-mail address: paul.glover@nottingham.ac.uk (P.M. Glover).

1090-7807/$ - see front matter © 2005 Elsevier Inc. All rights reserved.
doi:10.1016/j.jmr.2005.05.021

A major use of such software packages is the design of combustion chambers for turbines or furnaces. A methane combustion model is built into the CFD software package used herein and, therefore, may be used to support the findings of the imaging experiment.

The Single Point Ramped Imaging with T_1 Enhancement (SPRITE) technique is described elsewhere in greater detail [9]. The SPRITE family of techniques is highly suitable for imaging of materials with very short T_1 and T_2^* or, in this case, fast flowing gases exhibiting a short effective T_2^* due to turbulence or dispersion. These latter two effects are more fully explored by Newling et al. [8]. Briefly, only a single point of k-space is acquired for each RF pulse (although see below for a variation upon this basic theme). The gradient used to encode the location of the point in k-space is switched prior to the RF pulse and is maintained during both pulse and subsequent signal acquisition. SPRITE is, therefore, a purely phase encoded imaging technique. The single point is acquired typically at only 150 μs after the RF pulse. This time interval is usually termed t_p. A low tip angle is usually used because of the rapid repetition of the pulses.

The image contrast for the SPRITE method depends largely on the T_1 of the sample and the driven steady-state equilibrium magnetisation following a train of pulses. The SNR per unit imaging time may be optimised by careful choice of RF flip angle [10]. The advantage of SPRITE is evident in materials imaging where short T_1 and T_2^* relaxation times are common. For methane at STP the T_1 is 23 ms and the T_2 is 21 ms. Hence SPRITE would require only very low angle pulses be used. However, in the case of fast moving gas (up to 2 m s^{-1} in this case) travelling through the probe volume (having length 20 mm), a single proton may only experience a few RF pulses if a TR of a few milliseconds is used. SPRITE for gas flow can therefore accept a higher level of RF pulse amplitude than that usually calculated from the Ernst angle relationship. Mass transport will inevitably affect the form of the MRI signal [2]. In this particular experiment, however, t_p is sufficiently short that flow and dispersion, which lead to phase dispersion and hence signal attenuation in conventional imaging, have a reduced effect upon image intensity [8]. Therefore, the SPRITE pixel intensity is closer to the proton magnetisation density than that of conventional MRI methods. In using SPRITE any chemical shift information is lost. However, we are unable to see any water vapour signal and therefore our images are purely from methane gas.

This paper describes the design of a cooled probe which is suitable for NMR combustion studies having a relatively high calorific output. A water cooling system is employed to keep the loop-gap resonator mechanically stable and minimise tuning drift. A methane gas jet provides the fuel which is delivered to the burning chamber enclosed by the probe. A copper extractor hood removes fumes from the probe and magnet bore.

2. Methods

2.1. Probe design

There is always an upper limit to the temperature at which an NMR probe can operate. This limit is usually determined by the materials used for construction and the components used for tuning the probe. Most polymers soften at less than 450 K and solder will liquefy at around 550 K. Unlike X-band ESR measurements which employ a mechanically tuned cavity, capacitors are usually soldered directly onto a tuned NMR probe. Hence de-tuning due to temperature coefficients of the capacitors, destruction of the components, or melting of the solder joints would be likely during operation at elevated (flame) temperatures. Heating would change the geometry (and hence inductance) of self-supported simple wound coils making it difficult to maintain the tuning of a probe to resonance.

An NMR probe for combustion studies therefore requires either some protection from the heat of the process or some cooling mechanism. Thermal insulation and other cooling methods only serve to reduce filling factor and hence reduce sensitivity. In addition, it is undesirable to deliver water cooling directly to the probe coil itself because of the need to avoid signal pick up, which may be possible for conductors carrying the RF circuit currents and water internally. As such a low proton density is being imaged, it is essential to reduce the likelihood of spurious signal pickup. Gas flow cooling was also rejected because of the need to maintain a steady flame and hence the overall complexity of glasswork required would be increased dramatically. Usually, in MRI, it is also desirable to avoid metal structures and plates as these give rise to eddy currents and distort the images. However, the SPRITE imaging method is largely immune to such effects (again, by virtue of the short encoding time) and large area metal structures can be used within the gradient set, allowing the incorporation of a heat sink into the probe design. Gravity and the need to vent combustion products will necessarily govern the geometry of any probe for combustion studies. While a high field vertical bore magnet lends itself very easily to the combustion aspects, a horizontal bore magnet was the only one available having an adequate bore diameter. A loop-gap resonator design has therefore been chosen even though at 100 MHz this arrangement will not be optimal in terms of RF performance.

A simplistic argument can be used to show that a good filling factor is more desirable than keeping a low probe temperature for best sensitivity. Noise will

be proportional to the square-root of probe absolute temperature and the signal per voxel will fall approximately with the volume of the probe. Clearly the overall SNR depends on the relationship between volume and temperature rise caused by the sample. The heating due to radiation is balanced by the rate at which heat is conducted away to a heat sink. For a centrally located source such as a flame where much of the heat is carried away by convection—as small a probe diameter as possible is advantageous. However, it is the flame dynamics which will determine the diameter of the flame enclosure. A viable flame in a tube requires a minimum tube diameter due to gas expansion.

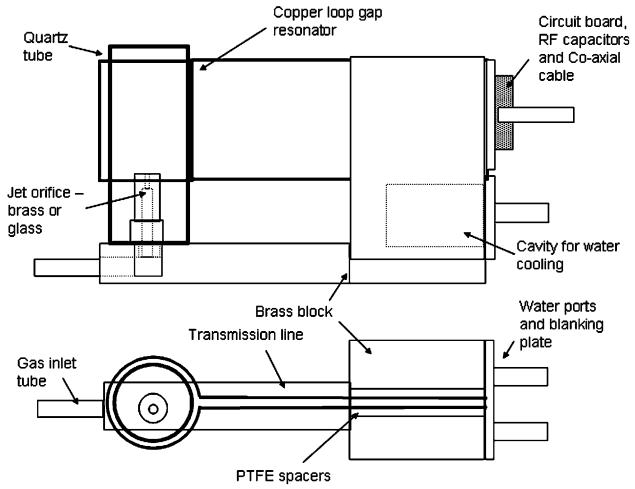

Fig. 1. Diagrams showing probe construction in both elevation and plan.

Fig. 1 shows the layout of the probe and Fig. 2 shows photographs of the probe. The loop-gap resonator (20 mm long × 18 mm diameter) encloses a quartz glass tube which has an inner diameter of 16 mm. The latter acts as a chimney where air is sucked in from the base of the tube and hot gases are exhausted from the top into a fume hood. Both the single-point imaging and projection reconstruction methods used in this study are techniques which are relatively insensitive to eddy currents. These methods therefore allow the use of a heat sink, consisting of a solid metal sheet and block, within the probe, which would usually give rise to image artifacts in MRI. The 100 MHz loop-gap resonator is connected to the tuning components via a two-plate transmission line which passes through a cooled brass block. Clearly, a multi-turn solenoidal probe would give better sensitivity. However, mechanical stability would

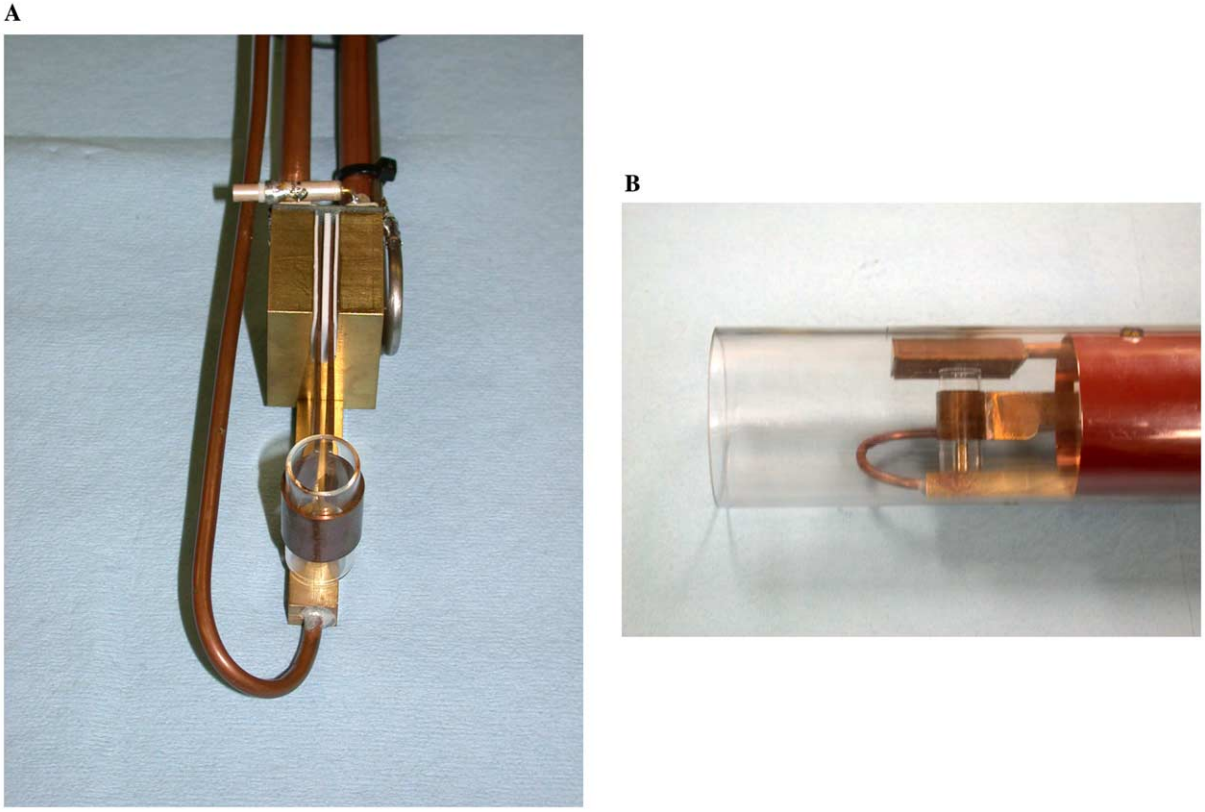

Fig. 2. Photographs of probe: (A) showing end view with gas inlet and loop-gap resonator enclosing quartz tube. (B) The probe mounted in 75 mm diameter poly-carbonate tube. The fume hood above the flame and part of the thin copper sheet RF screen can be seen. During operation a further RF screen is present which reduces RF coupling to the gradients as well as assisting in distributing any heat away from the hood area.

be difficult to achieve, leading to tuning drift. A 15 μs RF pulse was required for a 90° pulse at 50 W RF power. The transmission-line plates are insulated from the block by PTFE sheet which serves two functions. First it acts as a conductor of heat—although usually regarded as an insulator it is sufficiently thin that it keeps the copper cool enough to prevent damage to the RF capacitors mounted on the back of the block. Second it partially tunes the resonator, and parallel capacitance here will not degrade the performance of the probe. A circuit board is mounted on the block to carry the discrete tuning and matching components. The probe is connected to the spectrometer pre-amplifier via a rigid non-magnetic coaxial cable having a PTFE dielectric. A circuit diagram of the probe is shown in Fig. 3. The good thermal contact between capacitors and cooled block ensures that the tuning is not compromised during high temperature operation. No re-tuning of the probe was required between lit and unlit gas flow. No difference in baseline thermal (Johnson) noise was observed when the flame was lit or when the probe was at room temperature. The whole probe assembly was sheathed in a thin sheet copper RF screen and placed inside a 75 mm o.d. poly-carbonate tube suitable for insertion into the Nalorac micro-imaging gradient set.

2.2. Gas delivery apparatus

Pure methane gas is delivered to the probe burner through a cylinder regulator set to 2.5 p.s.i. and an Atheson rotameter flowmeter (No. 610) and needle valve as shown in Fig. 4. The flow gauge reading was corrected for methane and the controlled range was from 50 to 100 ml min^{-1}. The un-mixed gas was delivered via either a 1 mm diameter orifice in a 5 mm diameter cutting brass ($CuZn_{40}Pb_2$) nozzle or from a glass tube of 1 mm i.d. and 2 mm o.d. For a methane flame of about 20 mm height a gas flow rate of 80 ml min^{-1} was used, giving a nominal mean gas velocity leaving the hole of 1.7 m s^{-1}. A copper fume extractor hood was mounted over the top of the glass tube and attached to a roughing pump via a vapour trap and needle valve.

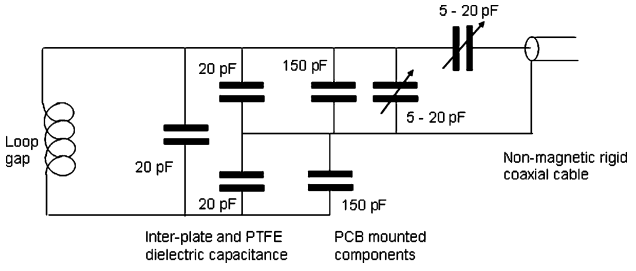

Fig. 3. Circuit diagram of probe circuit showing both physical capacitors and effective capacitance between the plates and block.

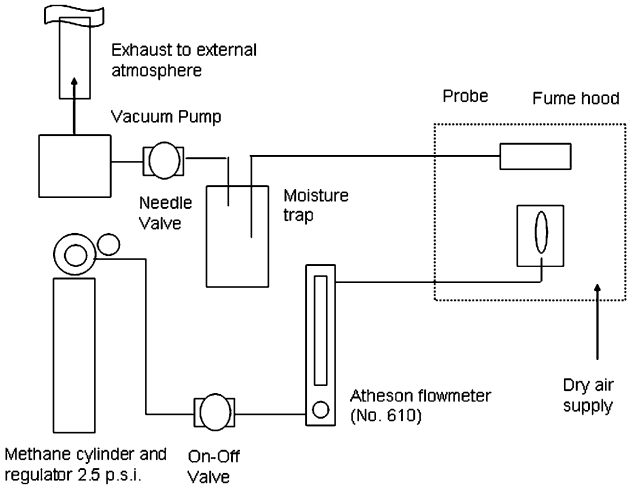

Fig. 4. Gas flow supply and control for flame. Also shown is fume extraction and exhaust system.

The extraction rate was set such that the flame was just on the point of being visibly affected by the draught from the hood. A supply of dry (2% RH) air is introduced at the sealed end of the magnet bore which ensured that no condensation formed on the RF components giving rise to spurious signal. The probe was sufficiently sensitive that signal from normal humid air (40% RH) within the probe could be observed easily, when there was no combustion and the dry air supply was off. No remote method of lighting the flame was provided. The flame was lit with the probe removed from the polycarbonate tube and outside the magnet. The probe was reinserted into the tube and then into the magnet with the flame lit. The equilibrium temperature of the resonator part of the probe was reached in just a few minutes. The cooled parts of the probe (including the nozzle) were held within a few degrees of room temperature.

2.3. Experimental design

The spectrometer is based on a Tecmag Apollo system with an AMT RF amplifier, Miteq low noise preamplifier and three axis Techron gradient power supplies.

The imaging parameters were as follows. The RF pulse durations used were either 5 μs (tip angle 30°) or 10 μs (60°). The interval between RF pulse and the first single point acquisition was 150 μs. In a variation upon the basic SPRITE sequence, subsequent (multiple) points were sampled at a 6 μs sampling interval, for use in signal averaging to improve SNR per unit imaging time [10]. (Such a scheme may also be employed to characterise sample T_2^*.) A base, band filter bandwidth of 63 kHz was selected. A 32 step SPRITE ramp was used with 2 ms between steps and 32 steps in the second dimension. A peak gradient of 98 mT m^{-1} was used which gave a maximum field of view of 40 mm. The

overall delay between ramp cycles was 50 ms. Even at the fastest gas flow of 2 m s^{-1} at the orifice, the amount of intra-voxel de-phasing was minimal. Measurement of an effective T_2^* for the fastest flowing methane gave a typical value of around 700 μs. From the imaging parameters given here, the resultant images can be said to be close to the true spin density. Using the brass nozzle the total imaging time was 3 h (2500 averages) for the unlit flowing gas and 7.5 h for the flame images (a total of 6000 averages). Using the glass tube nozzle both lit and unlit acquisitions had 5000 averages taking 4.5 h each.

Two-dimensional imaging was carried out where the x-axis was a projection (i.e., no slice has been selected). The z-axis was horizontal (magnet axis) and y-axis was vertical. In the work described here, up to 32 points were acquired for each RF excitation. Each of the 32 points will yield a pure phase encoded image but with a different field of view—scaling with effective t_p value for that image. The images are then mapped back onto a single field of view image using a chirp Z-transform (CZT) [11], which is described in greater detail by Halse et al. [10].

Computational modelling of methane gas flow has been carried out using a simplified model of the orifice in order to make comparisons with images. The geometry of the brass orifice was modelled in CADKEY (Release 2, CADKEY, MA, USA) and imported into the CFD package (CFX, Release 5.5, AEAT Technology, Ontario, Canada). A built-in methane–air combustion model was used to simulate the gas flow within the flame and visualise the combustion products in CFX. The geometry was meshed by hand, with approximately 90% smaller mesh size near the orifice and in the area directly surrounding the combustion than at the outskirts of the geometry. Automatic mesh adaptation was carried out as the simulation was run. To mimic the conditions of the MRI measurement, in particular the fume hood, a slight negative pressure was applied at the top of the tube. This generated an up-draught of 0.05–0.1 ms^{-1}.

3. Results

Initial examinations of the free induction decay (FID) from both lit and unlit gas showed a signal with T_2^* values of between 150 and 700 μs (lit) and 4–10 ms (unlit). The level of signal in the case of the lit gas was just discernible above the noise for 2 min of averaging. A short component of signal was present which came from the area of the circuit board, over 80 mm away from the iso-centre and 25 kHz off resonance. This signal, probably from the epoxy used in the circuit board itself, caused an artifact within the images, but because of the nature of multiple point SPRITE, its spatial position varied with t_p. The artifact could therefore be removed easily and images in which it overlapped the gas jet were discarded.

The images (1.25 mm resolution) of four different experimental conditions are shown in Fig. 5. The images are projections onto a vertical–axial plane, i.e., they are YZ images with the X plane averaged. The images show both lit and unlit cases for the two designs of orifice. The gas jet orifice is at the base of the image. The glass tube orifice (Fig. 5B) produces a narrow jet of gas which only disperses laterally by a small factor whereas the brass orifice shows much greater dispersion (Fig. 5A). Both gas flow rates are identical, but the brass orifice only narrows to 1 mm internal diameter for the last 3 mm of its length. Before this point the inlet is 2.5 mm i.d. The total length of glass tube is 20 mm in its holder, has a 1 mm i.d. along its whole length and thus produces flow of a different character. Visually, the flame produced by each orifice was similar, except for the diameter of the 'neck' of the flame, i.e., the blue ring at the base of the flame about 1 mm above the orifice. This ring was approximately the diameter of the plate around the orifice, about 2 mm in the case of the glass and 4 mm in the case of the brass.

The images in Figs. 5B and D show the effect of lighting the gas. The nuclear magnetisation associated with protons emerging from the orifice are entirely extinguished within a few millimeters of travel. In the case of the glass tube, the methane can be seen in the tube

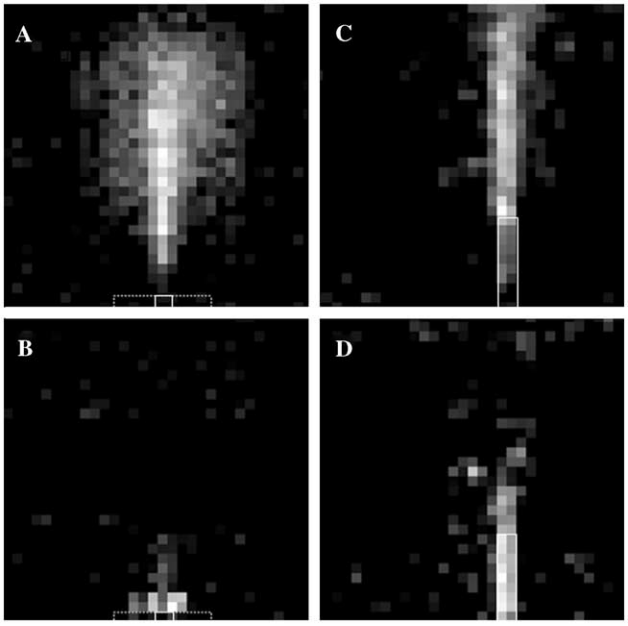

Fig. 5. SPRITE multiple point images showing: (A) unlit jet from brass nozzle and (B) the lit jet. Images taken using the glass tube nozzle showing the (C) unlit jet and (D) the lit gas. The solid white outlines show the size of the nozzle orifice (containing un-burnt gas) in each case. The broken white outlines show the solid brass disc, which surrounds the brass nozzle.

but decays away quickly except for the presence of a small signal about 3 mm into the flame. These are the remnants of un-dissociated methane within the outer borders of the flame. The effective T_2^* can be determined from FID data to be less than 200 μs. Evidence for this result can be seen in the bulk decay characteristic of plume and flame gas (where unburnt methane gives a smaller, but visible FID). These decay data are shown in Fig. 6. Examination of image in Fig. 5B shows a small jet into the flame and a bright disk under the flame neck and above the orifice which appears to flare like a trumpet bell. A number of factors lead to the conclusion that this is a disk of gas spreading laterally across the diameter of the orifice plate, rather than any signal from a deposit on the plate. This effect is only seen when the flame is burning. Any deposited layer is very thin and, as the RF magnetic field is necessarily perpendicular to the plate, then it would be difficult to see anything on the surface. The nozzle does not get particularly hot as the brass block underneath is held at the cooling water temperature. Visual inspection indicates oxidised/corroded brass at the plate, rather than proton containing compounds. No analysis has been carried out, but a small deposit of paramagnetic copper compounds (oxides or carbonates) could easily account for the small phase shift in the signal seen in the gas at this point. Indeed the brass susceptibility could in itself introduce a 1 kHz shift, which is of the right order. The T_2^* at this point would reflect that of cool gas, akin to that measured for the plumes.

For non-flowing gases with a longer effective T_2^* due to lower flow velocity (e.g., propane, for which T_2 is on the order of 490 ms), imaging methods such as projection reconstruction (PR) would be an obvious choice. For comparison with the SPRITE images, a spin-echo PR image of flowing propane gas with TE = 1 ms is shown in Fig. 7. The base of the unlit plume is not visible at all and only the slowed gas in the main body of the tube can be seen. The nozzle velocity of the propane was one quarter that of methane, chosen to give a sustainable flame when lit. By re-scaling Fig. 5A, it is possible to see that methane gas does re-circulate around the whole tube, in the same way as the propane, and it is this component of the mixture which dominates the spin-echo image.

Fig. 8 shows the results of CFD calculations for the flame above the brass nozzle geometry. Fig. 8A suggests that the methane has burnt completely (mass fraction falls to zero) within 2 cm of the orifice in the vertical. The figure also suggests a lateral spreading

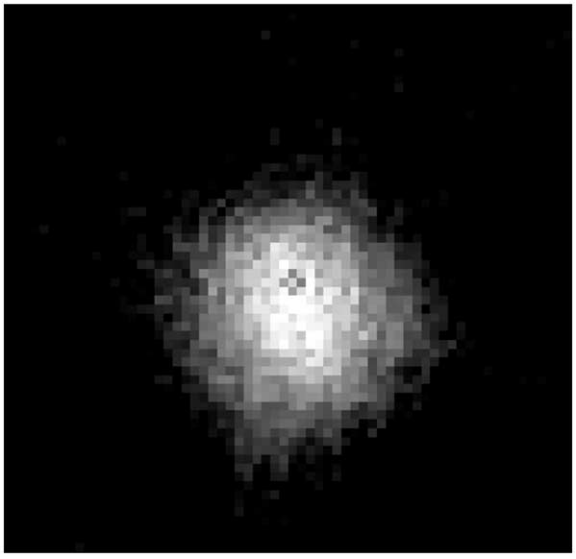

Fig. 7. Projection reconstruction image of unlit propane gas from brass nozzle at 20 ml min^{-1}. The nozzle is at the bottom of the picture. The image was constructed using the Shepp-Logan back projection filter.

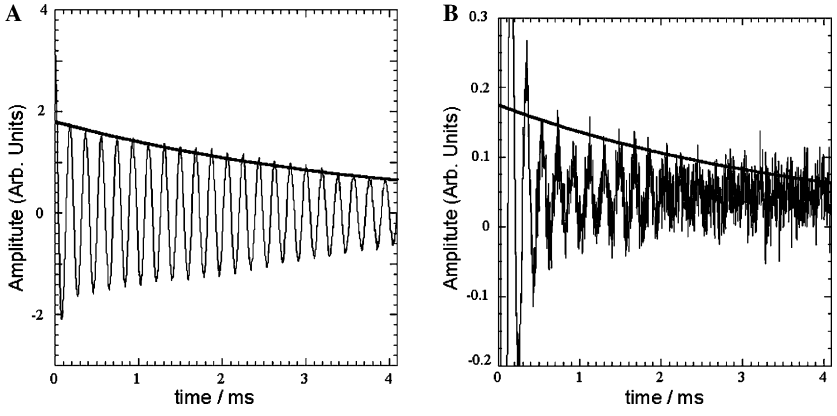

Fig. 6. Free induction decays of: (A) unlit propane gas plume and (B) the propane flame, in which some un-burnt gas signal is detected. In both FIDs, there is some signal with a much shorter time constant than that of the gas, which is associated with the material of the probe assembly. The thicker solid line is the signal model $S_0 \exp(-t/4\text{ ms})$. The ordinate on both graphs is the signal intensity in arbitrary units; (B) is scaled by a factor of 14 compared to (A).

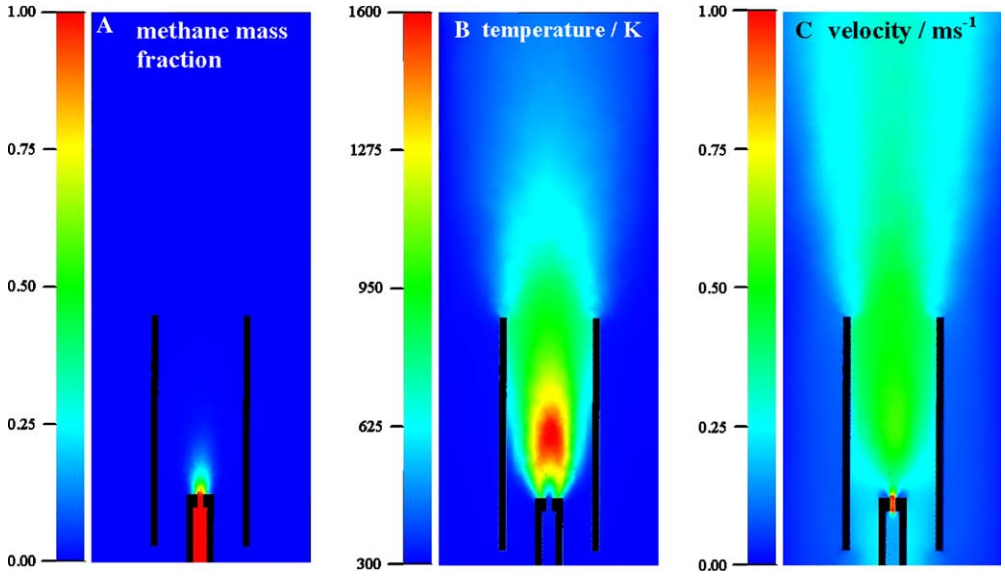

Fig. 8. CFD simulation of flame for comparison with image of the lit gas from the brass nozzle (seen in Fig. 5B).

of the un-burnt gas across the face of the brass plate, which exactly mirrors the interpretation of the MR image in Fig. 5B. The unburnt gas visible in Fig. 5B is certainly at elevated temperature, perhaps on the order of 600 K by comparison with the calculations of Fig. 8B. The boundary conditions of the CFD calculation were selected such that the nozzle speed of methane gas was 1 m s^{-1} for comparison with the MR measurements (Fig. 8C).

4. Conclusions

This paper describes the design of a novel cooled probe based on the loop-gap resonator which is suitable for very high temperature MRI studies. It is specifically designed for use with single point imaging methods as large areas of metal are present. However, the use of other imaging methods such as projection reconstruction are not precluded, but only slow moving gas can be successfully imaged. The probe used here for gas flow and flame studies may be used for other combustion studies where the calorific output is quite high. The thermal noise level and probe de-tuning were not affected unduly with this design. This design of probe has been used at 100 MHz which is at the lower end of its efficient usable range. Such a system would perform even better at higher field strengths. The sensitivity of this probe would increase at higher frequencies (up to around 300 MHz where the capacitance of the PTFE plates would start to dominate). The axial homogeneity of the magnet used caused the small number of residual protons contained in the circuit board to be observed—emphasising the need for very careful design when extended RF circuits are employed. Variations on the probe described here can be envisaged for both higher frequency and vertical bore magnets. The latter would be the preferred option and this will be the subject of future work involving a seed gas which will report on combustion but not combusted or disassociated in the flame.

In this paper, fast gas flow from a small orifice has been imaged for the first time. Images show the (unsurprising) result that the gas maintains its jet like nature for more laminar flow from the glass tube. The more turbulent flow coming from the brass nozzle results in a plume-like structure. The images where the gas is lit show un-disassociated methane in only up to 3 mm from the orifice, but within the flame itself. The methane is disassociated above 800 K and the resulting free radicals destroy any magnetisation. A lateral spreading of gas at the orifice is observed when the brass nozzle is used—as the flame has a neck as wide as the diameter of the nozzle plate. Molecular water is not observed higher up in the flame, because either the high temperature of the combustion products results in low available magnetisation, the density is far too low, or fast removal from the probe precludes polarisation of the water molecules (which have a long T_1 compared to methane).

Acknowledgments

We wish to acknowledge the advice and assistance of Murray Olive, Brian Titus, and Rod MacGregor during the construction of the probe system. P.M.G. wishes to thank B.J.B. for the opportunity to visit UNB; the UK EPSRC for a travel grant (GR/S56061) and the University of Nottingham for study leave.

References

[1] N.-K. Bär, F. Bauer, D.M. Ruthven, B.J. Balcom, Direct and indirect observation of coke deposits on HZSM-5 by ^{1}H NMR imaging, J. Catal. 208 (2002) 224–228.
[2] P.T. Callaghan, Principles of magnetic resonance microscopy, Clarendon Press, Oxford, 1991.
[3] A. Tkac, Free-radicals in the gas-phase—ESR investigation of flame and microwave plasma of atomised gases—a contribution to flame retardation and polymer erosion mechanisms, Polym. Degrad. Stabil. 33 (2) (1991) 171–206.
[4] N.M. Marinov, W.J. Pitz, C.K. Westbrook, A.M. Vincitore, M.J. Castaldi, S.M. Senkan, C.F. Melius, Aromatic and polycyclic aromatic hydrocarbon formation in a laminar premixed *n*-butane flame, Combust. Flame 114 (1998) 192–213.
[5] R. Bombach, B. Käppeli, Simultaneous visualisation of transient species in flames by planar-laser-induced fluorescence using a single laser system, Appl. Phys. B 68 (1999) 251–255.
[6] G. Papadopoulos, R.A. Bryant, W.M. Pitts, Flow characterization of flickering methane/air diffusion flames using particle image velocimetry, Exp. Fluids 33 (3) (2002) 472–481.
[7] B. Newling, S. Gibbs, J. Derbyshire, D. Xing, L. Hall, D. Haycock, W. Frith, S. Ablett, Comparison of MRI velocimetry with computational fluid dynamics, J. Fluids Eng. 119 (1997) 103–109.
[8] B. Newling, C.C. Poirier, Y. Zhi, J.A. Rioux, A.J. Coristine, D. Roach, B.J. Balcom, Velocity imaging of highly turbulent gas flow, Phys. Rev. Lett. 93 (15): Art. No. 154503, October 8, 2004.
[9] B.J. Balcom, R.P. MacGregor, S.D. Beyea, D.P. Green, R.L. Armstrong, T.W. Bremner, Single point ramped imaging with T1 enhancement (SPRITE), J. Magn. Reson. A 123 (1996) 131–134.
[10] M. Halse, J. Rioux, S. Romanzetti, J. Kaffanke, B. MacMillan, I. Mastikhin, N.J. Shah, E. Aubanel, B.J. Balcom, Centric scan SPRITE magnetic resonance imaging: optimization of SNR, resolution and relaxation time mapping, J. Magn. Reson. 169 (2004) 102–117.
[11] O. Heid, Sensitivity enhanced single point imaging, in: Proceedings of the 6th Annual Meeting of the International Society of Magnetic Resonance in Medicine, 1998, p. 2186.